https://doi.org/10.5194/egusphere-2024-3581
Preprint. Discussion started: 2 December 2024

Exploring the Aerosol Activation Properties in a Coastal Area Using Cloud and Particle-resolving Models

Ge Yu[1], Yueya Wang[2], Zhe Wang[2], Xiaoming Shi[2]

[1]Division of Emerging Interdisciplinary Areas, Hong Kong University of Science and Technology, Hong Kong, China
[2]Division of Environment and Sustainability, Hong Kong University of Science and Technology, Hong Kong, China

Correspondence to: Xiaoming Shi (shixm@ust.hk)

Abstract. Aerosols significantly impact the global climate by affecting the Earth's radiative balance and cloud formation. However, conducting high-altitude aerosol observations is currently costly and challenging, leading to gaps in accurately assessing aerosol activation properties during cloud formation. In this study, the Cloud Model 1 (CM1) is employed to investigate the movement of air parcels under shallow convection conditions in a coastal area. Subsequently, the evolution of various aerosol populations in the ideal scenarios is simulated by the PartMC-MOSAIC model to investigate their activation properties. It is found that leaving the boundary layer and entering the free atmosphere causes environmental changes in the parcels, which in turn alter the aerosol evolution and the cloud-forming potential. The impact of ascent timing is notably manifested in the concentration of ammonium nitrate rather than other chemical constituents. The rapid formation of ammonium nitrate accelerates the aerosol aging process, thereby modifying the hygroscopicity of the population. The differences between the aerosol populations in the boundary layer and high altitudes highlight the necessity of vertical observations and numerical modeling. In addition, as supersaturation rises from 0.1% to 1%, the relative discrepancy in cloud condensation nuclei (CCN) activation ratio between the particle-resolved results and the internal mixing assumption increases from 7% to 30%. This emphasizes the potential of appropriate mixing state parameterization in assessing aerosol activation properties. This study advances the understanding of aerosol hygroscopic changes under real weather conditions and offers insights into future modeling of aerosol-cloud microphysics.

1 Introduction

Atmospheric aerosols play an important role in the global climate by influencing the Earth's radiative balance and cloud formation. They also have a large effect on visibility, human health, and air quality (Mishra et al., 2023). Aerosols originate from both natural sources and anthropogenic sources. Once they enter the atmosphere, these diverse aerosols can have a long lifespan, undergoing various transport and aging processes. The diverse sources and complex evolution processes lead aerosols to exhibit various physical and chemical characteristics (Calvo et al., 2013). Consequently, aerosols display a complex spectrum, and affect the climate by scattering and absorbing shortwave radiation (Curtis et al., 2017). In addition to their radiative effects, some aerosols serve as cloud condensation nuclei (CCN) and participate in the cloud formation process (Charlson et al., 1992). These clouds can reflect sunlight and absorb terrestrial radiation, resulting in heating or cooling impacts,

https://doi.org/10.5194/egusphere-2024-3581
Preprint. Discussion started: 2 December 2024

thereby affecting the climate. However, the interactions between aerosols and clouds remain uncertain, complicating the climate research inquiries (Graf, 2004; Lolli, 2023).

In the process of cloud formation, CCN plays a crucial role by acting as the initial site where water vapor condenses to form cloud droplets (McFiggans et al., 2006; Motos et al., 2023; Alexandri et al., 2024). When an air parcel containing aerosols encounters a supersaturated environment, a portion of the particles can be activated and act as CCN to form cloud droplets (Pöhlker et al., 2021; Reutter et al., 2009). The specific proportion of the activated particles, known as the CCN activation ratio, can reflect the cloud-forming effectiveness of the aerosol population under a given supersaturation. It is an important indicator when studying the role of aerosols in cloud formation and their subsequent impacts on the Earth's climate system. The κ-Köhler theory (Köhler, 1936; Petters and Kreidenweis, 2007) was introduced and developed to calculate whether an aerosol particle can be activated into a CCN based on its size and composition. To investigate the CCN activity, it is critical to trace the hygroscopicity parameter κ, an intuitive and widely used factor to indicate the water uptake capacity of the aerosols. Many studies have revealed a direct correlation between hygroscopic behavior and the chemical composition of aerosols. Specifically, the mixtures of inorganic ions, organic matter, black carbon, and mineral dust constitute the majority of ambient aerosols (Jurányi et al., 2010). The hygroscopic behavior of the single-component aerosols such as sulfate and sodium chloride has been thoroughly investigated (Petters and Kreidenweis, 2007; Topping et al., 2005). In turn, aerosols with homogeneous composition have been studied extensively. However, ambient aerosol populations always consist of complex mixtures with varying geometric sizes, chemical compositions, and mixing states (McFiggans et al., 2006; Mikhailov et al., 2009; Swietlicki et al., 2008), which may collectively influence their hygroscopicity and CCN activity. Comprehending aerosol contributions to cloud formation necessitates the investigation of the particle evolution in the atmosphere. However, quantifying hygroscopic behavior remains challenging due to the spatial, temporal, and compositional complexity of aerosol particles (Rosenfeld et al., 2014).

Experimental studies have established a critical foundation for studying the variability of aerosol hygroscopicity and CCN activity. Aerosol parameters influencing CCN activity, such as size and chemical composition, are measured concurrently for specific samples. In field research, CCN closure studies compare predicted CCN activities with direct measurements. For instance, Juranyi et al. (2010) measured CCN number concentrations at a remote high-alpine research station. Combining dry number size distribution data from a scanning mobility particle sizer (SMPS) and bulk chemical composition data from an aerosol mass spectrometer (AMS) and a multi-angle absorption photometer (MAAP), the closure study showed good agreement, emphasizing the importance of the mean chemical composition. However, the prediction of CCN using bulk chemical composition data does not align with the measurement in every station. Moore et al. (2012) reported large discrepancies in hygroscopic coefficients derived from size-resolved aerosol composition and size-averaged data. Simplifications in mixing state and composition could lead to 35% to 75% CCN overpredictions. In certain cases in California, applying the externally mixed assumption or utilizing size-resolved data improved closure. Yeung et al. (2014) utilized a Humidified Tandem Differential Mobility Analyzer (HTDMA) and an Aerodyne High-Resolution Time-of-Flight Aerosol

https://doi.org/10.5194/egusphere-2024-3581
Preprint. Discussion started: 2 December 2024

Mass Spectrometer (HR-ToF-AMS) to report aerosol hygroscopicity and size-resolved composition at a coastal suburban site in Hong Kong for the first time. Closure was achieved by assuming the dominant effect of sulfate. Hansen et al. (2015) indicated that κ values decrease with increasing dry particle diameters for all studied chemical components, suggesting that κ-HTDMA depends on particle diameter and/or surface effects. Cai et al. (2018) found that better agreement between calculated and measured CCN activation ratios could be achieved by adjusting the surface tension based on the particle size, highlighting the critical role of particle size distribution in estimating water uptake properties. Fan et al. (2020) delved into the influence of aerosol aging processes on particle hygroscopic coefficients, stressing the importance of measuring the effective density and morphology of ambient black carbon (BC) in regions affected by rapid aerosol aging. Pure BC particles, being largely insoluble, are generally considered less relevant for CCN activation (Kuwata et al., 2009), while the impacts of mixed BC aerosols on cloud microphysical properties are still of great interest (Ching et al., 2016; Sarangi et al., 2019). In summary, field studies have greatly enhanced our understanding of real-world aerosol populations; nevertheless, these studies face limitations due to constraints in instrument placement and sample availability. Experimentally, the average κ is typically estimated from bulk chemical measurements as the κ of individual particles is difficult to get. The simplifications sometimes result in nonnegligible errors in CCN calculations (Meng et al., 2014). This is because the mixing state of the aerosols cannot reach the two ideal extremes defined by the literature (Winkler, 1973), either externally mixed or internally mixed. While particle compositions can sometimes be measured within specific size bins, identifying the precise composition of individual particles experimentally remains difficult. Besides, hygroscopicity studies in environments with complex meteorological changes, such as high altitude, are challenging to implement due to limited portability of instruments including CCN counters (CCNCs).

This necessitates the development of numerical modeling tools to investigate aerosol evolution and distribution patterns. One particle-resolved model named as Particle Monte Carlo model (PartMC) was introduced as an effective tool to address this significant challenge (Riemer et al., 2009). PartMC is a comprehensive model that accounts for the composition and size of each single computational particle. The researchers have also coupled it with the modern Model for Simulating Aerosol Interactions and Chemistry (MOSAIC) to deterministically treat the gas-phase and gas-to-particle questions (Zaveri et al., 2008). Leveraging its particle-based approach, the PartMC-MOSAIC model can be used to explore how different mixing state assumptions influence the evolution of aerosol populations in complex environments. A series of studies employed this model to study the related impacts of the black carbon mixing state on processes such as nucleation scavenging and cloud processing (Beeler et al., 2022; Ching et al., 2012). Tian et al. (2014) investigated the evolution of ship-emitted aerosol particles and validated the model with observations from the QUANTIFY study in 2007. Plume-exit modeling was conducted by Mena et. al (2017) to investigate the CCN activity of aerosols from residential biofuel combustion. This model has shown potential to be applied in various scenarios to help interpret the CCN measurement (Razafindrambinina et al., 2023). Additionally, the model can calculate the mixing state index defined based on the Shannon entropy (Riemer and West, 2013), facilitating studies on the significance of mixing state in CCN activity (Ching et al., 2017, 2019; Zheng et al., 2021). Despite its advantages, few studies have applied this model in aerosol research to investigate the transition of air parcels leaving the boundary layer.

https://doi.org/10.5194/egusphere-2024-3581
Preprint. Discussion started: 2 December 2024

Previous work did not consider the movement of parcels under actual meteorological conditions, limiting the accurate representation of environmental conditions when studying the cloud-forming ability of aerosols in a prolonged evolution. Furthermore, prior studies suggest that aerosol hygroscopic properties are significantly affected by long-term aging processes.

To address these issues, the cloud model 1 (CM1) is applied in this study to initially investigate the movement characteristics of air parcels under a shallow cumulus convection condition. Key parameters obtained from the CM1 experiments and observations are then introduced into the PartMC-MOSAIC model to investigate the evolution of aerosol populations across different air parcel scenarios. By analyzing key indicators such as hygroscopicity, critical supersaturation, and mixing state index, this study explores the cloud-forming abilities of aerosols within different parcels.

2 Methodology

In this study, we designed several ideal scenarios resembling parcels in the coastal area under a typical shallow cumulus weather condition. For each parcel, the evolution of the aerosols is investigated with a detailed particle-resolved model. The relevant characteristics of the particles in different scenarios are also comprehensively analyzed to compare the cloud-forming potential of the aerosol populations.

2.1 Different scenarios

In coastal areas, clouds tend to form at relatively low altitudes. Under shallow cumulus convection, the ascending height of air parcels originating from near-surface levels can range from a few hundred meters to several thousand meters, reaching the altitude where cloud formation occurs. We utilized the Cloud Model 1 (CM1) (Bryan and Fritsch, 2002) to perform large-eddy simulations of ideal shallow cumulus convection conditions. During the simulation, we employed tracers to track 484 parcels originating from near-surface levels, in conjunction with the other background settings. After a 6-hour simulation period, we analyzed the vertical positions of all tracked parcels. Approximately one-third (182 parcels in our simulation) of the parcels ascended to altitudes exceeding 1000 meters. The ascending time of the parcels exhibited a wide range of variability and was not constrained within specific time limits. Some particles exhibited vertical height fluctuations near the surface, while many others remained at higher altitudes after the updraft brought them into the free troposphere for several hours. The ascent speed of the parcels was relatively fast, typically taking between 8 to 20 minutes to reach altitudes exceeding 1000 meters from a near-surface height. We selected representative ascending and surface-dwelling parcels and extracted their temperature, pressure, kinetic diffusion coefficients, and other related information for subsequent scenario setups.

In **Supplementary Information 1**, the vertical distributions of some basic environmental variables in the CM1 experiment are shown. From Fig. S1, significant environmental changes occur at altitudes above 500 meters. Clouds have already formed at the locations where many parcels can reach. Due to the randomness in ascent times of the parcels and the differences between the surface and higher altitudes, we designed four scenarios for the box model as follows,

https://doi.org/10.5194/egusphere-2024-3581
Preprint. Discussion started: 2 December 2024

Scenario A: the parcel remains near the ground.

Scenario B: the parcel ascends to a high altitude 2 hours after the initialization.

Scenario C: the parcel ascends to a high altitude 6 hours after the initialization.

Scenario D: the parcel ascends to a high altitude 10 hours after the initialization.

The initialization was finished after the 6-hour spin-up simulations, which is detailed described in subsection 2.2. For the parcels that stay at the surface, the background temperature was set to 26 ℃ (299 K), and the pressure was set to the standard atmospheric pressure. After updraft, the temperature rapidly dropped to 17 ℃ (290 K) and the pressure became 880 hPa, approximately 1.2 km. Besides, the horizontal eddy diffusivity at the high altitude was about one-fifth of the value near the surface.

After obtaining the updraft-related settings from the 9-hour CM1 results, we consulted other sources to refine the long-time scenario configuration. The background conditions including the diurnal changes in mixing height and the emission data were derived from the idealized plume scenario settings conducted by Riemer et al. (Riemer et al., 2009). The aerosol data at the surface was obtained from the observations at a general air quality monitoring station in Hong Kong (Wang and Yu, 2017). With the MERRA-2 (the Modern-Era Retrospective Analysis for Research and Applications, Version 2) reanalysis data, the different concentration ratios of various aerosol species at the ground level and high altitude were estimated in coastal areas. After that, the ground-level measurements were converted to the high-altitude background aerosol data. Detailed information on the number concentration and size distribution of the aerosols in different modes can be found in Table 1. The initial aerosol conditions contain three modes that are the same as the Ground part because all the parcels stay near the surface during the initialization period.

Table 1. Aerosol conditions for the emissions (Riemer et al., 2009) and different backgrounds.

	N (m^{-3})	D_{gm} (μm)	σ_g	Composition by Mass
Emissions				
Meat cooking	9×10^6	0.0865	1.9	100% OC
Diesel vehicles	1.6×10^8	0.05	1.7	30% OC, 70% BC
Gasoline vehicles	5×10^7	0.05	1.7	80% OC, 20%BC
Ground				
Condensation	1.26×10^9	0.0816	1.6	32.6% BC, 48.8% OC, 14% SO_4, 5.6% NH_4
Droplet	2.68×10^8	0.14	2.1	26.4% BC, 23.8% OC, 37.4% SO_4, 11.2% NH_4, 0.4% Cl, 0.7% NO_3
Coarse	2.3×10^5	2.16	1.65	11.8% BC, 21% OC, 12.2% SO_4, 0.5% NH_4, 17.8% Cl, 18.6% NO_3, 18.1% Na
High altitude				

https://doi.org/10.5194/egusphere-2024-3581
Preprint. Discussion started: 2 December 2024

Condensation	3.1×10^8	0.0831	1.66	15.8% BC, 44.5% OC, 29.8% SO_4, 9.9% NH_4
Droplet	6.8×10^7	0.16	2.05	9.1% BC, 15.5% OC, 57.1% SO_4, 17.2% NH_4, 0.1% Cl, 1% NO_3
Coarse	6.6×10^4	2.16	1.64	5.7% BC, 19.1% OC, 25.8% SO_4, 1% NH_4, 4.4% Cl, 39.6% NO_3, 4.4% Na

2.2 PartMC simulations

The coupled PartMC-MOSAIC model was applied in this study to simulate the evolution of the individual aerosols in a Lagrangian air parcel (Riemer et al., 2009; Zaveri et al., 2008). PartMC is a 0-D box model and could resolve the specific size and composition of the remaining particles inside the computational volume. The volume used is about a few cubic centimeters and well mixed, which represents a larger parcel suspended in specific scenarios. Instead of tracking the physical positions, the model focuses on monitoring the number, mass, and full composition distributions of the simulated particles (Zaveri et al., 2010). When the parcel leaves the exhaust source, no freshly emitted particles and gas will be added to the computational volume. Aside from the emission module, the number concentration of the particles is also impacted by the dilution, and coagulation processes that are stochastically calculated in the PartMC model. Within the box model, the meteorological conditions and gas concentrations are assumed to be homogeneous. When coupled with the MOSAIC model, some other processes such as condensation, evaporation, and chemical reactions can be included in the simulation. MOSAIC consists of modules for gas-phase photochemistry (Zaveri and Peters, 1999), particle-phase thermodynamics (Zaveri et al., 2005), and gas-particle mass transfer (Zaveri et al., 2008). With these modules, the model could treat a total of 77 gas species and the atmospherically important aerosol species like sulfate (SO_4), nitrate (NO_3), chloride (Cl), carbonate (CO_3), ammonium (NH_4), sodium (Na), calcium (Ca), methane sulfonic acid (MSA), black carbon (BC), primary organic aerosol (OC), and several secondary organic aerosol (SOA) species. A more detailed description of the governing equations and numerical methods used in the model is given in Riemer et al. (2009).

We used PartMC version 2.6.1 for this study and initialized the number of computational particles as 10^5. The time step of the simulation was 60 seconds. The simulations were conducted for 30 hours. The first 6-hour simulation (from 0:00 a.m. to 6:00 a.m.) is used for the spin-up process, and the subsequent 24-hour simulation (from 6:00 a.m. to 6:00 a.m. on the next day) is employed to analyze the diurnal variation of the aerosols.

2.3 CCN activity computation

To quantitatively assess the cloud-forming potential of an aerosol population, we could investigate the CCN activity at a specific supersaturation level. The factor is a straightforward proportion between activatable CCN particles and the total aerosol particles (CN, condensation nuclei). PartMC-MOSAIC could provide useful information about each particle, allowing us to calculate the hygroscopicity value (κ) and subsequently determine the critical supersaturation (S_c) required for activation.

https://doi.org/10.5194/egusphere-2024-3581
Preprint. Discussion started: 2 December 2024

Hence, we could evaluate whether each particle is activated at a certain supersaturation with the S_c and get the CCN/CN ratio (CCN activity).

The hygroscopicity parameter κ_i of the particle i, as introduced by Ghan et al. (2001), and Petters and Kreidenweis (2007), is a dimensionless parameter to reflect the water uptake property of the aerosol. The water activity $a_{w,i}$ of the particle i is given by,

$$\frac{1}{a_{w,i}} = 1 + \kappa_i \frac{V_{dry,i}}{V_{w,i}} \tag{1}$$

where $V_{dry,i}$ is the dry particle volume and $V_{w,i}$ is the volume of water in the particle. For the particle i containing various components, κ_i is the volume-weighted average of the κ values of its constituent aerosol species. Table 2 lists κ values assigned to different species simulated in this study (Clegg et al., 1998; Riemer et al., 2009; Zaveri et al., 2010).

The equilibrium saturation ratio $S_i(D_i)$ over an aqueous droplet is given by the following Köhler equation:

$$S_i(D_i) = a_{w,i} \exp\left(\frac{4\sigma_w M_w}{RT\rho_w D_i}\right) \tag{2}$$

where σ_w is the surface tension of the water-air interface, M_w is the molecular weight of the water, R is the universal gas constant, T is the temperature, ρ_w is the density of water, and D_i is the wet diameter of the particle. Combining the equations and using the D_i and the dry diameter $D_{dry,i}$ to replace the respective volumes, we obtain the κ-Köhler equation introduced by Petters and Kreidenweis (2007),

$$S_i(D_i) = \frac{D_i^3 - D_{dry,i}^3}{D_i^3 - D_{dry,i}^3(1-\kappa_i)} \exp\left(\frac{4\sigma_w M_w}{RT\rho_w D_i}\right) \tag{3}$$

We could compute the critical wet diameter $D_{c,i}$ first and then calculate the critical supersaturation ratio $S_{c,i}$. We may set the $\partial S_i(D_i)/\partial D_i$ to zero to numerically solve the $D_{c,i}$ at which $S_i(D_i)$ is maximal. Substituting the $D_{c,i}$ into the equation and $S_{c,i}$ equals $(S_i(D_{c,i}) - 1)$ percent. Once the $S_{c,i}$ is equal to or less than the environmental supersaturation, the CCN-active aerosols could be identified and counted.

Table 2. Hygroscopicity parameters were assigned to the species used in the study.

Aerosol species	κ
NO_3	0.65
SO_4	0.65
NH_4	0.65
Na	1.1
Cl	1.1

https://doi.org/10.5194/egusphere-2024-3581
Preprint. Discussion started: 2 December 2024

BC	0
OC	0.001
SOA	0.1

3 Results for the aerosol activation properties

3.1 The changes in the aerosol chemical compositions

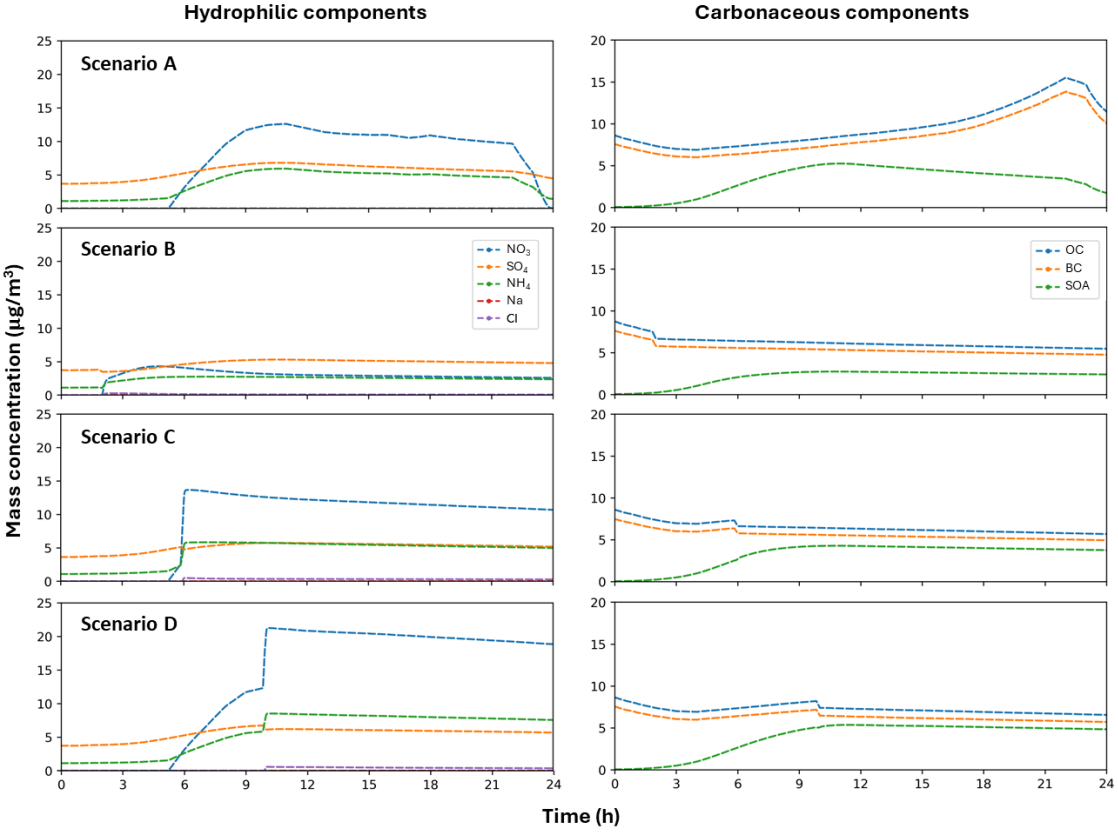

Figure 1. Mass concentration variations over time of hydrophilic and carbonaceous components in Scenario A, B, C, and D.

Starting from this section, we analyze the results from the PartMC-MOSAIC simulations. The aerosol data of the PartMC parcels representing the four scenarios are extracted and plotted separately. To evaluate the sources, transport, and transformations of the substances in these aerosol populations, the mass concentration variations of the hydrophilic and carbonaceous components in aerosols are investigated, as shown in Fig. 1. In the coastal area, the main components of hydrophilic aerosols include sulfate, nitrate, ammonium ions, and sea salt, which corresponds to relatively higher hygroscopicity parameters κ. Among these components, the concentration changes of ammonium and nitrate are the most pronounced across different scenarios. The mass concentration of sulfate generally hovers around 5 μg/m³. By contrast, the

https://doi.org/10.5194/egusphere-2024-3581
Preprint. Discussion started: 2 December 2024

content of sodium and chloride is relatively low, not exceeding 1 μg/m³ in all simulation cases. Specifically, the parcel containing aerosols in Scenario A remains below the boundary layer, where temperature and humidity are stable. As mentioned in the methodology, the time analyzed throughout this section starts at 6:00 AM (0th hour). Therefore, after 9:00 AM (the 3rd hour in the figures), the influence of sunlight and anthropogenic emissions leads to a significant increase in gas concentrations. The concentrations of ammonia (NH_3) and nitric acid (HNO_3) near the ground peak around the 5th hour due to gas emissions and photochemical reactions, facilitating the conversion to ammonium nitrate (NH_4NO_3) and promoting the growth of new particles. After the 21st hour, the combination of decreased emission and enhanced dilution accounts for the reduction in the mass concentration of the aerosols. In Scenarios B, C, and D, the parcel rises at the 2nd, 6th, and 10th hour respectively, corresponding to the rapid decrease in the temperature and pressure. According to the equilibrium reactions introduced in the MOSAIC model, the gas-particle transfer processes for nitrate and ammonium ions are sensitive to temperature changes, leading to a rapid increase in nitrate and ammonium ion concentrations. Specifically, in Scenario B, the early ascent brings the parcel to a relatively clean environment before sunlight and anthropogenic factors significantly influence the gas substances. Hence, the concentration of the ammonium nitrate does not exhibit the same pronounced changes as in the other two scenarios. The detailed and clear mass changes during the two hours around the parcel ascent are shown in **Supplementary Information 2**.

The emissions cease after the air parcel leaves the boundary layer and reaches higher altitudes. However, the diffusion effect persists although it weakens. Due to the absence of fresh precursors and the background with lower aerosol concentration, the concentrations of ammonium and nitrate ions gradually decline. Meanwhile, as the duration of emissions increases for parcels that stay in the boundary layer for a longer time, the peak concentration of ammonium nitrate significantly rises. Specifically, the peak concentration of ammonium nitrate in Scenario D is approximately 4 times that of Scenario B.

Carbonaceous components include BC, OC, and SOA. They exhibit lower hygroscopicity (κ) values compared to hydrophilic components. In Scenario A, the mass concentration of OC and BC steadily increases due to the accumulation of urban emissions from the 3rd to 21st hour, as seen in Fig. 1. Their concentrations start to decline after the 21st hour due to decreased emissions and increased dilution. Differently, the mass concentration of SOA is decreased after the 11th hour because of the cessation of the transformation from OC to SOA. When the parcel rises above the boundary layer, the concentrations of OC and BC are predominantly influenced by the dilution module rather than emission sources as seen in Scenarios B, C, and D. The formation of SOA is primarily driven by light exposure, exhibiting a variation pattern generally consistent with Scenario A. Besides, the specific peak concentrations of SOA increase as the emission accumulates.

https://doi.org/10.5194/egusphere-2024-3581
Preprint. Discussion started: 2 December 2024

3.2 The evolution of hygroscopicity in different scenarios

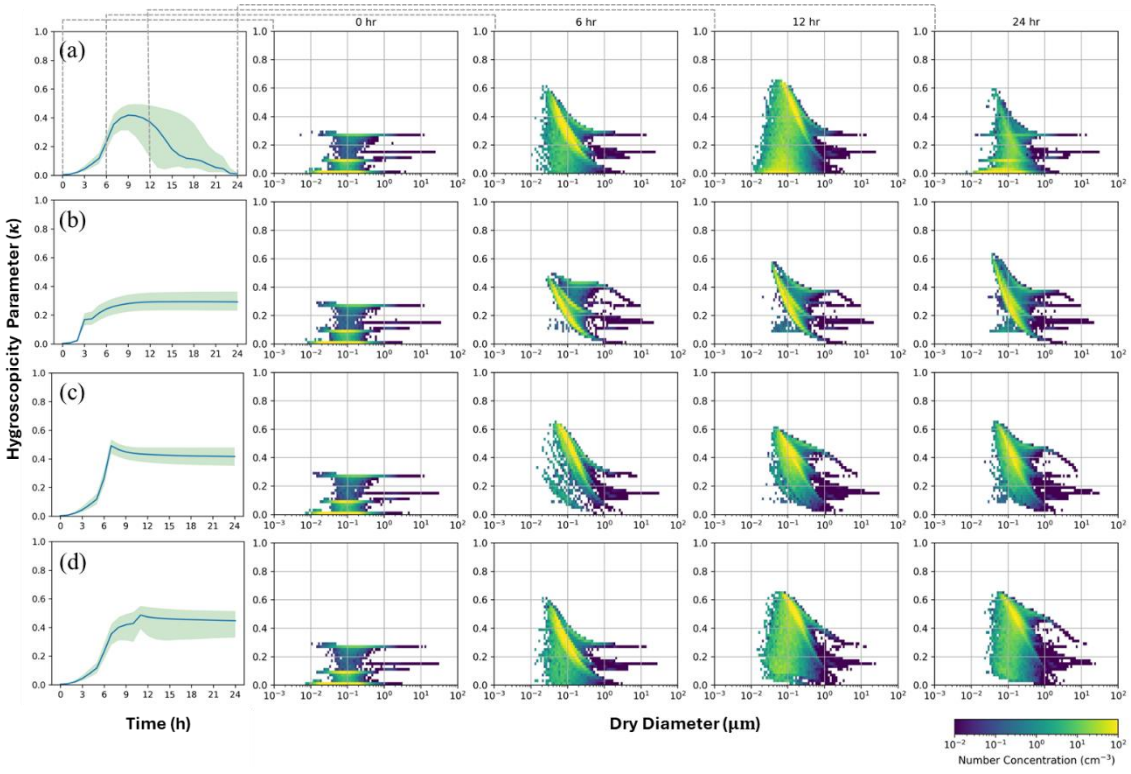

Figure 2. The hygroscopicity parameter changes over time and the number concentration distribution of the particles with different κ values across particle size at 0, 6, 12, and 24 hours in (a) Scenario A, (b) Scenario B, (c) Scenario C, and (d) Scenario D. The blue solid line in the left plots represents the median κ across the aerosol population, while the edges of the green shading denote the 25th and 75th percentile κ values.

Figure 2 illustrates the evolution of the hygroscopicity parameter κ over time and the selected particle-resolved hygroscopicity distribution versus particle size in four different scenarios. In Scenario A, the median κ value rises during the initial 9 hours and then gradually declines over the subsequent 15 hours. Such trends align closely with the variation of the hydrophilic components, especially sulfate, nitrate, and ammonium. By contrast, in Scenarios B, C, and D, the ascent of the parcel corresponds to an increase in the median κ. This is because the updraft process results in a rapid decrease in the temperature and pressure, which speeds up the gas-to-particle conversion process, thereby accelerating the formation of hygroscopic chemical components. In addition, due to the absence of an emission term and the reduced diffusion effect, the median κ and the overall distribution remain relatively stable after the parcel ascends to high altitudes.

Aside from the hygroscopicity parameter κ, the particle size also influences the activation properties of aerosols as described in section 2.3. Thus, the number concentration distribution of the particles with different κ values across particle size is also depicted in the subplots of Fig. 2. The temporal changes of the aerosol size distribution under different scenarios are directly shown in **Supplementary Information 3**. From Fig. S3, the average size of the aerosol populations becomes larger with time

https://doi.org/10.5194/egusphere-2024-3581
Preprint. Discussion started: 2 December 2024

owing to the condensation and coagulation processes. This aging process of the aerosols could also be seen from the subplots in Fig. 2, where the yellow portion representing high-concentration aerosols shifts towards larger particle sizes.

Regarding the specific hygroscopicity distribution with the particle size, it is evident that all the scenarios share a similar pattern at the very beginning of the simulation shown in the second column of Fig. 2. The bright yellow part predominates the population because of the large number concentration. On the 0th hour, there are three bright lines parallel to the x-axis representing the three sub-populations of the initial aerosol conditions mentioned in section 2.1. The sub-population at $\kappa \approx 0$ comes from the fresh emissions mainly consisting of the black carbon and the primary organic carbon. The other two sub-populations at the hygroscopicity around 0.1 and 0.3 bring the features of the background mixture containing ammonium, sulfate, nitrate, sea salt, aged black carbon, and organic carbon. As time passes by, the sub-populations characterized by bright yellow have exhibited an increased hygroscopicity, which is attributed to the aging process of black carbon and the formation of ammonium nitrate. This phenomenon is evident in the third column, which depicts the distribution for the 6th hour. In Scenario B, the parcel has been stationed at a high altitude after the 2nd hour and shows a lower aging level compared to others. Conversely, in Scenario C, the ascent process of the parcel has accelerated the aging process, thus influencing the predominant sub-population to a higher κ distribution by the 6th hour. After that, the patterns in Scenario B and C keep their features and both the aerosol populations experience a similar aging process. On the 12th hour, the aerosols in Scenario D retain many original features after the parcel rises. However, in Scenario A, a significant proportion is occupied by freshly emitted hydrophobic particles. After sunset, it becomes difficult for accumulated pollutants to disperse. Furthermore, the aging process has also slowed down owing to reduced photochemical reactions. Over the last 3 hours, the sub-populations with high hygroscopicity have gradually diminished in Scenario A. This can be attributed to an intensified diffusion effect resulting from the changes in the mixing height.

https://doi.org/10.5194/egusphere-2024-3581
Preprint. Discussion started: 2 December 2024

3.3 Critical supersaturation distribution and CCN activation ratio

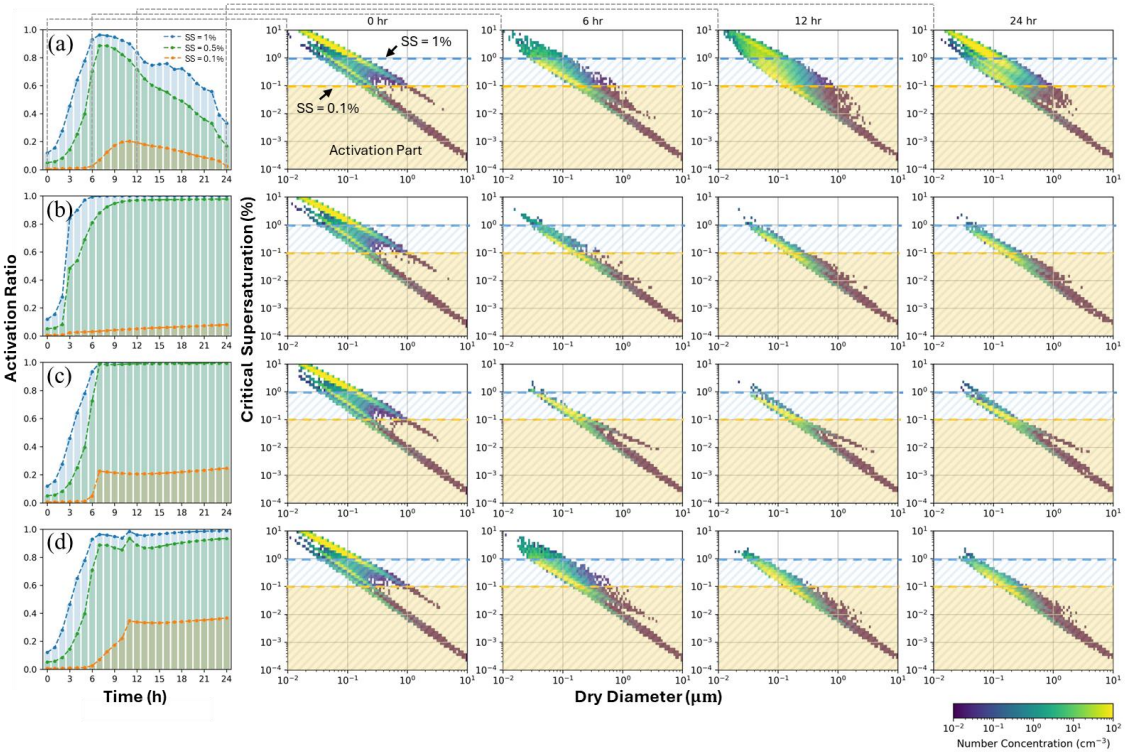

Figure 3. The temporal variations of CCN activity at 0.1%, 0.5%, and 1% supersaturation, as well as the critical supersaturation distribution across particle size at 0, 6, 12, and 24 hours in (a) Scenario A, (b) Scenario B, (c) Scenario C, and (d) Scenario D. The orange and blue horizontal dashed lines indicate supersaturations equaling 0.1% and 1%, respectively.

The right part of Fig. 3 shows the distribution of critical supersaturation (S_c) across particle dry diameter, at the same selected times as Fig. 2. As described in the methodology section, the critical supersaturation of each particle is a fundamental property that directly relates to its ability to become activated as a CCN. The horizontal dashed lines represent the supersaturation values equaling 0.1% and 1%. Below the lines are the particles that could be activated at this supersaturation and the color bar represents the number concentration. The value of S_c depends on the hygroscopic characteristic decided by all the mixed species and the dry diameter. When the diameter becomes larger, the overall trend of the critical supersaturation should become lower as per the Köhler formula. The dry diameter is not the only impacting factor, so the distribution of this value is not concentrated along a single line in the plot. The spread pattern is also largely affected by the heterogeneity of κ, which is determined by the chemical composition of the particles. The sensitive impacts of different compositions on the overall S_c are studied in **Supplementary Information 4**. It is observed that some hydrophilic species tend to form on smaller particles during the aging process, necessitating consideration of the specific mixing state when evaluating the activation properties of particles.

https://doi.org/10.5194/egusphere-2024-3581
Preprint. Discussion started: 2 December 2024

At the very beginning, the particles at 0.1 μm have the S_c ranging from 0.2% to 2%, and the S_c of most of them is higher than 1%. Besides, a large number of particles is smaller than 0.1 μm at this period. Therefore, the aerosol population exhibits a low activation potential since the supersaturation levels during cloud formation typically remain below 1%. At the 6th hour, the yellow portion in Scenario A and D has shifted to the lower part of the subplots. This is attributed to the overall increase in particle size and κ values observed in the majority of the particles. The range of S_c for most particles is between 0.1% and 1%, significantly influencing the activation ratio of the aerosol population within this range of supersaturation. In Scenario B and C, the earlier updraft process results in lower S_c levels for the bright yellow sub-populations. By the 12th hour, the characteristics of bright areas in scenarios B, C, and D, like the ones at the 6th hour, are largely preserved on the graph. The colored regions have reduced in size because of the dilution module. However, a significant portion of high S_c and small particles from the freshly emitted aerosols remains within the parcel of Scenario A. After sunset, the dilution process near the ground weakens, leading to a pronounced accumulation of pollutants. Until the 20th hour, the similar process continues. Combined with the diminished chemical conversion process caused by light conditions, the high S_c of most aerosols in Scenario A is noticeable at the 24th hour. At this time, the differences between parcels in three other scenarios and the parcel near the surface become more evident. The CCN activity either retains high or rapidly increases after ascending in the latter three scenarios. It is implied that these scenarios exhibit an enhancement in the ability of aerosols to act as CCN compared to the surface conditions after the 12th hour (in the nighttime).

The left column subplots of Fig. 3 compare the particle-resolved CCN activation ratio at 0.1%, 0.5%, and 1% supersaturation along with time between four scenarios. The gray dashed lines between the subplots represent the same time results. The colored curves on the left visually demonstrate the statistical outcomes that arise from the details of the S_c distribution presented on the right. Moreover, the trends observed in the colored curves for each scenario are consistent with the median κ depicted in Fig. 2.

https://doi.org/10.5194/egusphere-2024-3581
Preprint. Discussion started: 2 December 2024

4 Analysis of the mixing state in different scenarios

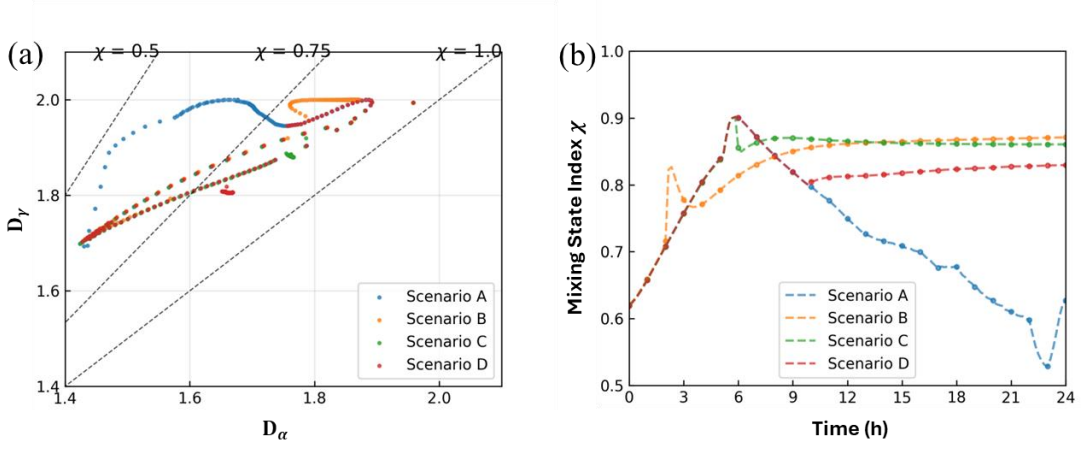

Figure 4. (a) Scatterplot showing the definition of the mixing state index χ for four scenarios. The scatters show the state of the average per-particle species diversity D_α and the bulk population species diversity D_γ at ten-minute intervals. (b) Temporal changes of the mixing state index χ for four scenarios. Every scatter represents the value for each hour.

In this work, we investigate the CCN prediction errors caused by the internally mixing state assumption by using the mixing state index (χ) concept proposed by (Riemer and West, 2013). In the state of fully external mixing ($\chi = 0$), each particle within the population possesses a distinct chemical composition. When χ is 1, it represents a state of fully internal mixing (all the particles have identical mass compositions).

Figure 4a shows the scatterplot of the average per-particle species diversity D_α and the bulk population species diversity D_γ at different times for various scenarios. According to the definition of the mixing state index χ, the index χ is an affine ratio of the D_α and the D_γ ($\chi = \frac{D_\alpha - 1}{D_\gamma - 1}$). The background aerosols are typically in a well-internally mixed state. Because of the different composition, the introduction of primary emissions may cause a decrease in the χ value. Besides, the process of physical or chemical aging naturally leads to an increase in the χ value of the aerosol population. Figure 4a presents the distribution of χ at 10-minute intervals and all the samples have a large value indicating more internally mixed. The χ value for the samples ranges from 0.5 to 1. In Scenario A, there is a larger amount of freshly emitted particles compared to the other scenarios due to the prolonged influx of emissions. Without the aging process, their compositions differ from the characteristics of the particles experiencing a lot of natural processes. As a result, some samples in Scenario A could exhibit a more externally mixing state and the χ value is lower than the other ones.

Figure 4b depicts the changes in the mixing state index of the four aerosol populations within 24 hours. It is evident that in the three scenarios where the parcel undergoes ascent, the χ value deviates from the curve in Scenario A after ascending. Notably, the aerosol population with lower pollution accumulation demonstrates an increasing trend in the χ value during the ascent, whereas the other two scenarios do not show a significant increase in the mixing state index. The observed trend in Scenario

https://doi.org/10.5194/egusphere-2024-3581
Preprint. Discussion started: 2 December 2024

B highlights the influence of aging level on the χ value. The deeper the aging level of the total population, the larger the mixing state index. To a certain extent, the changes in the χ value exhibit similar characteristics to the curves of the median κ value for every scenario. The primary emissions, dilution, chemical reactions, and other aging processes may have a similar impact on both the χ and κ values. All these processes can alter the specific chemical composition of particles, which in turn affects the general mixing state and hygroscopicity.

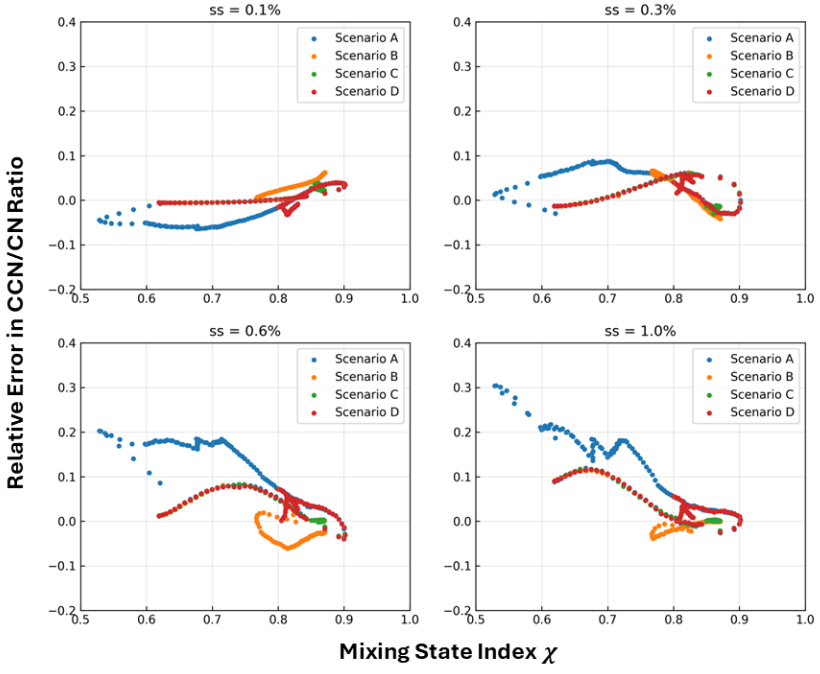

Figure 5. Relative errors in CCN activation caused by composition averaging with the mixing state index χ at different environmental supersaturations for four scenarios. The scatters show the results at ten-minute intervals.

Figure 5 presents the relationship between the composition averaging error in CCN activation with the mixing state index at different environmental supersaturations. Indeed, some models or measurement methods assume that the measured chemical composition mass is uniformly distributed within aerosol particles, which means a fully internally mixed state ($\chi = 1$). This assumption simplifies the calculations when estimating the hygroscopicity of the specific aerosol population and is widely used to investigate CCN activation. However, it is important to note that the actual mixing state of aerosol particles can deviate from this assumption, especially when the χ value is lower. In such cases, the aerosol population may exhibit a more non-uniform or externally mixed state, where different chemical components can exhibit significant differences among particles. When the supersaturation levels are 0.1% and 0.3%, the average relative error in CCN activation caused by composition averaging is less than 0.1. However, as the supersaturation levels increase to 0.6% and 1%, the CCN activation errors in some scenario samples may become larger. Specifically, in Scenario A, smaller χ values correspond to larger error values. The errors at a supersaturation level of 1% tend to be larger than those at a supersaturation level of 0.6%. This difference highlights that

https://doi.org/10.5194/egusphere-2024-3581
Preprint. Discussion started: 2 December 2024

when the mixing state is not as homogeneous, the assumption of internal mixing can lead to errors that exceed 10%. It underscores the importance of accurately determining the specific composition of particles to obtain more precise results. The deviation from the assumption of uniform mixing emphasizes the importance of employing accurate measurement techniques or particle-resolved models like PartMC-MOSAIC that can capture the real mixing state of aerosol particles. Such techniques can provide a more comprehensive understanding of the impact of the size distribution, chemical composition, and mixing state of the aerosols, thereby improving the accuracy of hygroscopicity calculations and related predictions.

5 Conclusion

Aerosol-cloud interactions remain a source of uncertainty in climate research. The current difficulty of high-altitude aerosol observations limits the investigation of the aerosol activation process at cloud-forming altitudes. The development of particle-resolving simulation tools, such as the PartMC-MOSAIC model, facilitates the quantitative analysis of the hygroscopic behavior and cloud-forming potential of the aerosol populations. However, the infrequent consideration of the meteorological effects of transporting the air parcels to high altitudes could also introduce some errors or misunderstandings. To bridge the gap, a combination of cloud and particle-resolving models is utilized to investigate the evolution and activation properties of aerosols under idealized scenarios.

In this study, CM1 was applied to capture movement characteristics of air parcels under a typical shallow cumulus convection condition. Four distinct scenarios were devised based on the CM1 experiment. The parcel in the basic scenario maintains stability near the surface, while the others ascend to cloud-forming altitudes at varying intervals. Critical parameters extracted from CM1 simulations, including temperature, pressure, and parcel ascent timing, were subsequently fed into the PartMC-MOSAIC model. The observational and reanalysis data in the coastal area were also incorporated for initialization. Compared to traditional frameworks, this PartMC-based approach offers a more comprehensive analysis of the specific chemical composition, hygroscopicity distribution, critical supersaturation distribution, and mixing state indices.

Following the ascent process into the free troposphere, aerosol-containing parcels cease to receive fresh emissions predominantly comprising hydrophobic substances and small particles. Rapidly ascending parcels may undergo significant environmental changes, such as a sharp temperature drop, impacting aerosol aging processes involving condensation and gas-to-particle conversion. In this study, the ammonium nitrate variation is noteworthy owing to its high sensitivity to the temperature. The accelerated formation of these hydrophilic species enhances aerosol aging, elevates the median hygroscopicity parameter κ of the aerosol population, and thereby impacts the particle activation properties. Compared to aerosol populations near the surface, those at high altitudes mostly display a higher CCN activation ratio. The absolute ratio difference can reach up to 66% at a supersaturation of 1%, emphasizing the influence of vertical transport on aerosol activation potential.

https://doi.org/10.5194/egusphere-2024-3581
Preprint. Discussion started: 2 December 2024

Moreover, scenarios with different parcel ascent timings reveal marked variations in hygroscopicity and particle size distributions, primarily due to various accumulations of aerosol precursors. These precursors, such as nitric acid gas, ammonia, and ozone, are influenced by emission factors and photochemical reactions. In Scenario B, the parcel ascends before emissions and sunlight can take an important role, and the population shows the minimal median and overall κ distribution among all the ascent scenarios. Hence, the cloud-forming potential is influenced by the ascent timing: the CCN activation in Scenario B could be as much as 15% lower than in the ground at a low supersaturation level (0.1%).

The combined consideration of the hygroscopicity and the size distribution is essential when estimating aerosol activation properties since some hydrophilic species may tend to form on smaller particles. The PartMC model is able to capture detailed particle-based chemical composition data, which could reduce CCN prediction inaccuracies associated with simplified mixing-state assumptions. In our study, the internal mixing-state assumption results in a relative error from 7% to 30% compared with the particle-resolved results as supersaturation ranges from 0.1% to 1%.

In summary, the integration of particle-resolving models with dynamic meteorological simulations could mitigate the limitations of size-resolved methods and compensate for the deficiencies in high-altitude observations. The differences in aerosol properties between high-altitude and ground-level parcels highlight the significance of vertical aerosol observations and numerical modeling. Additionally, the mixing state index has the potential to be accounted for in future climate models as it is still challenging to represent some microscale aerosol-cloud interactions and reduce the microphysical uncertainties in large-scale models.

Code/Data availability

The models used for the simulations, PartMC-MOSAIC and CM1, are open-source and can be obtained at https://github.com/compdyn/partmc and https://www2.mmm.ucar.edu/people/bryan/cm1/. The aerosol and gas data used in this study are freely available from papers listed in the Methodology section. The reanalysis dataset MERRA-2 is available at https://gmao.gsfc.nasa.gov/reanalysis/MERRA-2/. Other data is available after request.

Author Contribution

XS and GY conceptualized and designed the study. GY collected and processed the data and YW assisted in data processing. GY performed simulations, analyzed data, and wrote the original draft. ZW reviewed and contributed to the scientific discussions. XS supervised, reviewed, and edited the manuscript.

Competing Interests

The authors declare that they have no conflict of interest.

https://doi.org/10.5194/egusphere-2024-3581
Preprint. Discussion started: 2 December 2024

Acknowledgment

The work described in this paper was substantially supported by a grant from the Research Grants Council (RGC) of the Hong Kong Special Administrative Region, China (Project Reference: AoE/P-601/23-N). Additionally, XS by RGC grant HKUST-16307323. The authors thank HKUST Fok Ying Tung Research Institute and National Supercomputing Center in Guangzhou Nansha sub-center for providing high-performance computational resources.

References

Alexandri, F., Müller, F., Choudhury, G., Achtert, P., Seelig, T., and Tesche, M.: A cloud-by-cloud approach for studying aerosol–cloud interaction in satellite observations, Atmospheric Measurement Techniques, 17, 1739–1757, https://doi.org/10.5194/amt-17-1739-2024, 2024.

Beeler, P., Chakrabarty, R., Chen, J., China, S., Corbin, J., Mazzoleni, C., Shrivastava, M., Zaveri, R. A., Zelenyuk, A., and Fierce, L.: Simulating the evolution of black carbon mixing state through cloud processing with a particle-resolved model, 2022, A36E-09, 2022.

Bryan, G. H. and Fritsch, J. M.: A Benchmark Simulation for Moist Nonhydrostatic Numerical Models, 2002.

Cai, M., Tan, H., Chan, C. K., Qin, Y., Xu, H., Li, F., Schurman, M. I., Liu, L., and Zhao, J.: The size-resolved cloud condensation nuclei (CCN) activity and its prediction based on aerosol hygroscopicity and composition in the Pearl Delta River (PRD) region during wintertime 2014, Atmospheric Chemistry and Physics, 18, 16419–16437, https://doi.org/10.5194/acp-18-16419-2018, 2018.

Calvo, A. I., Alves, C., Castro, A., Pont, V., Vicente, A. M., and Fraile, R.: Research on aerosol sources and chemical composition: Past, current and emerging issues, Atmospheric Research, 120–121, 1–28, https://doi.org/10.1016/j.atmosres.2012.09.021, 2013.

Charlson, R. J., Schwartz, S. E., Hales, J. M., Cess, R. D., Coakley, J. A., Hansen, J. E., and Hofmann, D. J.: Climate Forcing by Anthropogenic Aerosols, Science, 255, 423–430, https://doi.org/10.1126/science.255.5043.423, 1992.

Ching, J., Riemer, N., and West, M.: Impacts of black carbon mixing state on black carbon nucleation scavenging: Insights from a particle-resolved model, J. Geophys. Res., 117, 2012JD018269, https://doi.org/10.1029/2012JD018269, 2012.

Ching, J., Zaveri, R. A., Easter, R. C., Riemer, N., and Fast, J. D.: A three-dimensional sectional representation of aerosol mixing state for simulating optical properties and cloud condensation nuclei, JGR Atmospheres, 121, 5912–5929, https://doi.org/10.1002/2015JD024323, 2016.

Ching, J., Fast, J., West, M., and Riemer, N.: Metrics to quantify the importance of mixing state for CCN activity, Atmospheric Chemistry and Physics, 17, 7445–7458, https://doi.org/10.5194/acp-17-7445-2017, 2017.

Ching, J., Adachi, K., Zaizen, Y., Igarashi, Y., and Kajino, M.: Aerosol mixing state revealed by transmission electron microscopy pertaining to cloud formation and human airway deposition, npj Clim Atmos Sci, 2, 22, https://doi.org/10.1038/s41612-019-0081-9, 2019.

Clegg, S. L., Brimblecombe, P., and Wexler, A. S.: Thermodynamic Model of the System H+−NH4+−SO42-−NO3-−H2O at Tropospheric Temperatures, J. Phys. Chem. A, 102, 2137–2154, https://doi.org/10.1021/jp973042r, 1998.

Curtis, J. H., Riemer, N., and West, M.: A single-column particle-resolved model for simulating the vertical distribution of aerosol mixing state: WRF-PartMC-MOSAIC-SCM v1.0, Geoscientific Model Development, 10, 4057–4079, https://doi.org/10.5194/gmd-10-4057-2017, 2017.

https://doi.org/10.5194/egusphere-2024-3581
Preprint. Discussion started: 2 December 2024

Fan, X., Liu, J., Zhang, F., Chen, L., Collins, D., Xu, W., Jin, X., Ren, J., Wang, Y., Wu, H., Li, S., Sun, Y., and Li, Z.: Contrasting size-resolved hygroscopicity of fine particles derived by HTDMA and HR-ToF-AMS measurements between summer and winter in Beijing: the impacts of aerosol aging and local emissions, Atmospheric Chemistry and Physics, 20, 915–929, https://doi.org/10.5194/acp-20-915-2020, 2020.

Ghan, S., Laulainen, N., Easter, R., Wagener, R., Nemesure, S., Chapman, E., Zhang, Y., and Leung, R.: Evaluation of aerosol direct radiative forcing in MIRAGE, Journal of Geophysical Research: Atmospheres, 106, 5295–5316, https://doi.org/10.1029/2000JD900502, 2001.

Graf, H.-F.: The Complex Interaction of Aerosols and Clouds, Science, 303, 1309–1311, https://doi.org/10.1126/science.1094411, 2004.

Hansen, A. M. K., Hong, J., Raatikainen, T., Kristensen, K., Ylisirniö, A., Virtanen, A., Petäjä, T., Glasius, M., and Prisle, N. L.: Hygroscopic properties and cloud condensation nuclei activation of limonene-derived organosulfates and their mixtures with ammonium sulfate, Atmos. Chem. Phys., 15, 14071–14089, https://doi.org/10.5194/acp-15-14071-2015, 2015.

Jurányi, Z., Gysel, M., Weingartner, E., DeCarlo, P. F., Kammermann, L., and Baltensperger, U.: Measured and modelled cloud condensation nuclei number concentration at the high alpine site Jungfraujoch, Atmos. Chem. Phys., 10, 7891–7906, https://doi.org/10.5194/acp-10-7891-2010, 2010.

Köhler, H.: The nucleus in and the growth of hygroscopic droplets, Trans. Faraday Soc., 32, 1152–1161, https://doi.org/10.1039/TF9363201152, 1936.

Kuwata, M., Kondo, Y., and Takegawa, N.: Critical condensed mass for activation of black carbon as cloud condensation nuclei in Tokyo, Journal of Geophysical Research: Atmospheres, 114, https://doi.org/10.1029/2009JD012086, 2009.

Lolli, S.: Machine Learning Techniques for Vertical Lidar-Based Detection, Characterization, and Classification of Aerosols and Clouds: A Comprehensive Survey, Remote Sensing, 15, 4318, https://doi.org/10.3390/rs15174318, 2023.

McFiggans, G., Artaxo, P., Baltensperger, U., Coe, H., Facchini, M. C., Feingold, G., Fuzzi, S., Gysel, M., Laaksonen, A., Lohmann, U., Mentel, T. F., Murphy, D. M., O'Dowd, C. D., Snider, J. R., and Weingartner, E.: The effect of physical and chemical aerosol properties on warm cloud droplet activation, Atmospheric Chemistry and Physics, 6, 2593–2649, https://doi.org/10.5194/acp-6-2593-2006, 2006.

Mena, F., Bond, T. C., and Riemer, N.: Plume-exit modeling to determine cloud condensation nuclei activity of aerosols from residential biofuel combustion, Atmos. Chem. Phys., 17, 9399–9415, https://doi.org/10.5194/acp-17-9399-2017, 2017.

Meng, J. W., Yeung, M. C., Li, Y. J., Lee, B. Y. L., and Chan, C. K.: Size-resolved cloud condensation nuclei (CCN) activity and closure analysis at the HKUST Supersite in Hong Kong, Atmos. Chem. Phys., 14, 10267–10282, https://doi.org/10.5194/acp-14-10267-2014, 2014.

Mikhailov, E., Vlasenko, S., Martin, S. T., Koop, T., and Pöschl, U.: Amorphous and crystalline aerosol particles interacting with water vapor: conceptual framework and experimental evidence for restructuring, phase transitions and kinetic limitations, Atmospheric Chemistry and Physics, 9, 9491–9522, https://doi.org/10.5194/acp-9-9491-2009, 2009.

Mishra, M., Gulia, S., Shukla, N., Goyal, S. K., and Kulshrestha, U. C.: Review of Secondary Aerosol Formation and Its Contribution in Air Pollution Load of Delhi NCR, Water Air Soil Pollut, 234, 47, https://doi.org/10.1007/s11270-022-06047-0, 2023.

Moore, R. H., Cerully, K., Bahreini, R., Brock, C. A., Middlebrook, A. M., and Nenes, A.: Hygroscopicity and composition of California CCN during summer 2010, Journal of Geophysical Research: Atmospheres, 117, https://doi.org/10.1029/2011JD017352, 2012.

Motos, G., Freitas, G., Georgakaki, P., Wieder, J., Li, G., Aas, W., Lunder, C., Krejci, R., Pasquier, J. T., Henneberger, J., David, R. O., Ritter, C., Mohr, C., Zieger, P., and Nenes, A.: Aerosol and dynamical contributions to cloud droplet formation in Arctic low-level clouds, Atmospheric Chemistry and Physics, 23, 13941–13956, https://doi.org/10.5194/acp-23-13941-2023, 2023.

https://doi.org/10.5194/egusphere-2024-3581
Preprint. Discussion started: 2 December 2024

Petters, M. D. and Kreidenweis, S. M.: A single parameter representation of hygroscopic growth and cloud condensation nucleus activity, Atmospheric Chemistry and Physics, 7, 1961–1971, https://doi.org/10.5194/acp-7-1961-2007, 2007.

Pöhlker, M. L., Zhang, M., Campos Braga, R., Krüger, O. O., Pöschl, U., and Ervens, B.: Aitken mode particles as CCN in aerosol- and updraft-sensitive regimes of cloud droplet formation, Atmospheric Chemistry and Physics, 21, 11723–11740, https://doi.org/10.5194/acp-21-11723-2021, 2021.

Razafindrambinina, P. N., Malek, K. A., De, A., Gohil, K., Riemer, N., and Asa-Awuku, A. A.: Using particle-resolved aerosol model simulations to guide the interpretations of cloud condensation nuclei experimental data, Aerosol Science and Technology, 57, 608–618, https://doi.org/10.1080/02786826.2023.2202741, 2023.

Reutter, P., Su, H., Trentmann, J., Simmel, M., Rose, D., Gunthe, S. S., Wernli, H., Andreae, M. O., and Pöschl, U.: Aerosol- and updraft-limited regimes of cloud droplet formation: influence of particle number, size and hygroscopicity on the activation of cloud condensation nuclei (CCN), Atmospheric Chemistry and Physics, 9, 7067–7080, https://doi.org/10.5194/acp-9-7067-2009, 2009.

Riemer, N. and West, M.: Quantifying aerosol mixing state with entropy and diversity measures, Atmospheric Chemistry and Physics, 13, 11423–11439, https://doi.org/10.5194/acp-13-11423-2013, 2013.

Riemer, N., West, M., Zaveri, R. A., and Easter, R. C.: Simulating the evolution of soot mixing state with a particle-resolved aerosol model, Journal of Geophysical Research: Atmospheres, 114, https://doi.org/10.1029/2008JD011073, 2009.

Rosenfeld, D., Sherwood, S., Wood, R., and Donner, L.: Climate Effects of Aerosol-Cloud Interactions, Science, 343, 379–380, https://doi.org/10.1126/science.1247490, 2014.

Sarangi, B., Ramachandran, S., Rajesh, T. A., and Dhaker, V. K.: Black carbon linked aerosol hygroscopic growth: Size and mixing state are crucial, Atmospheric Environment, 200, 110–118, https://doi.org/10.1016/j.atmosenv.2018.12.001, 2019.

Swietlicki, E., Hansson, H.-C., Hämeri, K., Svenningsson, B., Massling, A., McFiggans, G., McMurry, P. H., Petäjä, T., Tunved, P., Gysel, M., Topping, D., Weingartner, E., Baltensperger, U., Rissler, J., Wiedensohler, A., and Kulmala, M.: Hygroscopic properties of submicrometer atmospheric aerosol particles measured with H-TDMA instruments in various environments—a review, 60, 432–469, https://doi.org/10.1111/j.1600-0889.2008.00350.x, 2008.

Tian, J., Riemer, N., West, M., Pfaffenberger, L., Schlager, H., and Petzold, A.: Modeling the evolution of aerosol particles in a ship plume using PartMC-MOSAIC, Atmospheric Chemistry and Physics, 14, 5327–5347, https://doi.org/10.5194/acp-14-5327-2014, 2014.

Topping, D. O., McFiggans, G. B., and Coe, H.: A curved multi-component aerosol hygroscopicity model framework: Part 1 – Inorganic compounds, Atmospheric Chemistry and Physics, 5, 1205–1222, https://doi.org/10.5194/acp-5-1205-2005, 2005.

Wang, N. and Yu, J. Z.: Size distributions of hydrophilic and hydrophobic fractions of water-soluble organic carbon in an urban atmosphere in Hong Kong, Atmospheric Environment, 166, 110–119, https://doi.org/10.1016/j.atmosenv.2017.07.009, 2017.

Winkler, E. M.: Stone: Properties Durability in Man's Environment, Springer, Vienna, https://doi.org/10.1007/978-3-7091-4120-5, 1973.

Yeung, M. C., Lee, B. P., Li, Y. J., and Chan, C. K.: Simultaneous HTDMA and HR-ToF-AMS measurements at the HKUST Supersite in Hong Kong in 2011, JGR Atmospheres, 119, 9864–9883, https://doi.org/10.1002/2013JD021146, 2014.

Zaveri, R. A. and Peters, L. K.: A new lumped structure photochemical mechanism for large-scale applications, Journal of Geophysical Research: Atmospheres, 104, 30387–30415, https://doi.org/10.1029/1999JD900876, 1999.

Zaveri, R. A., Easter, R. C., and Peters, L. K.: A computationally efficient Multicomponent Equilibrium Solver for Aerosols (MESA), Journal of Geophysical Research: Atmospheres, 110, https://doi.org/10.1029/2004JD005618, 2005.

Zaveri, R. A., Easter, R. C., Fast, J. D., and Peters, L. K.: Model for Simulating Aerosol Interactions and Chemistry (MOSAIC), Journal of Geophysical Research: Atmospheres, 113, https://doi.org/10.1029/2007JD008782, 2008.

https://doi.org/10.5194/egusphere-2024-3581
Preprint. Discussion started: 2 December 2024

Zaveri, R. A., Barnard, J. C., Easter, R. C., Riemer, N., and West, M.: Particle-resolved simulation of aerosol size, composition, mixing state, and the associated optical and cloud condensation nuclei activation properties in an evolving urban plume, J. Geophys. Res., 115, 2009JD013616, https://doi.org/10.1029/2009JD013616, 2010.

Zheng, Z., West, M., Zhao, L., Ma, P.-L., Liu, X., and Riemer, N.: Quantifying the structural uncertainty of the aerosol mixing state representation in a modal model, Atmos. Chem. Phys., 21, 17727–17741, https://doi.org/10.5194/acp-21-17727-2021, 2021.